
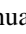
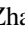


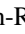
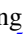
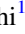






Lithium Evolution of Giant Stars Observed by LAMOST and Kepler

Jinghua Zhang¹ , Jian-Rong Shi^{1,2} , Hong-Liang Yan^{1,2} , Yaguang Li^{3,4} , Qi Gao^{1,2} , Chun-Qian Li^{1,2} ,
Xianfei Zhang⁵ , Shuai Liu^{1,2}, Shaolan Bi⁵ , Gang Zhao^{1,2} , and Yan Li^{2,6,7,8} 

¹ CAS Key Laboratory of Optical Astronomy, National Astronomical Observatories, Chinese Academy of Sciences, Beijing 100101, People's Republic of China
sjr@nao.cas.cn, hlyan@nao.cas.cn

² School of Astronomy and Space Science, University of Chinese Academy of Sciences, Beijing 100101, People's Republic of China

³ Sydney Institute for Astronomy (SfA), School of Physics, University of Sydney, NSW 2006, Australia

⁴ Stellar Astrophysics Centre, Department of Physics and Astronomy, Aarhus University, Ny Munkegade 120, DK-8000 Aarhus C, Denmark

⁵ Department of Astronomy, Beijing Normal University, Beijing 100875, People's Republic of China

⁶ Yunnan Observatories, Chinese Academy of Sciences, Kunming 650216, People's Republic of China

⁷ Key Laboratory for Structure and Evolution of Celestial Objects, Chinese Academy of Sciences, Kunming 650216, People's Republic of China

⁸ Center for Astronomical Mega-Science, Chinese Academy of Sciences, Beijing, 100012, People's Republic of China

Received 2021 June 10; revised 2021 August 26; accepted 2021 August 29; published 2021 September 20

Abstract

Mapping lithium evolution for evolved stars will provide restrictions and constraints on the fundamental stellar interior physical processes, which will shed further light on our understanding of the theory of stellar structure and evolution. Based on a sample of 1848 giants with known evolutionary phases and lithium abundances from the LAMOST-Kepler and LAMOST-K2 fields, we construct mass–radius diagrams to characterize the evolutionary features of lithium. The stars at red giant branch (RGB) phase show natural depletion along with their stellar evolution; particularly, there are no obvious crowd stars with anomalously high Li abundances near the bump. Most of the low-mass stars reaching their zero-age sequence of core helium burning (ZAHeB) have Li abundances around ~ 1.0 dex, which shows an increase of Li abundance by ~ 0.6 dex compared to the stars above the RGB bump. This suggests that helium flash may be responsible for moderate Li production, while for super Li-rich stars, some special mechanisms should be considered during helium flash. Other scenarios, such as mergers, could also be sources given that Li-rich stars can be found at any time during the steady-state phase of core He burning. During the core He-burning (HeB) phase, there is no indication of obvious lithium depletion.

Unified Astronomy Thesaurus concepts: [Stellar evolution \(1599\)](#); [Asteroseismology \(73\)](#); [Stellar abundances \(1577\)](#); [Lithium stars \(927\)](#); [Chemically peculiar stars \(226\)](#); [Red giant stars \(1372\)](#); [Red giant clump \(1370\)](#)

1. Introduction

Surface lithium abundances display various patterns for stars of different types as well as at different evolutionary stages. Lithium is easily destroyed by nuclear reactions in stars and it is sensitive to mixing events connecting the envelope with warm layers where it easily undergoes p-captures. Thus, the surface Li has experienced depletion over time for stars with convective envelopes (Twarog et al. 2020; Randich & Magrini 2021). Therefore, the signatures of Li are good manifestations of subtle physical processes beneath the surface and provide key information about internal stellar structure and evolution.

During the past few decades, increasing observational results have confirmed theoretical predictions about the depletion of Li in giant stars (e.g., Lind et al. 2009; Deliyannis et al. 2019; Twarog et al. 2020). However, due to the difficulties of classifying evolutionary stages, especially separating core helium burning (HeB) from red giant branch (RGB) bump stars by traditional approach, the evolutionary features of Li from the RGB to the HeB stage are still in the dark. Moreover, the nature of Li-rich giants found in a small number of objects is still beyond the standard stellar evolution theory (e.g., Wallerstein & Sneden 1982; Smiljanic et al. 2018; Yan et al. 2018; Casey et al. 2019; Deepak & Reddy 2019; Gao et al. 2019; Martell et al. 2021). The physical mechanisms responsible for those Li-rich giants are under debate (e.g., Charbonnel & Lagarde 2010; Kumar et al. 2020; Schwab 2020; Zhang et al. 2020; Mori et al. 2021; Singh et al. 2021; Yan et al. 2021), which further complicates Li evolution in evolved stars.

Fortunately, the asteroseismic analysis for a mass of giants in the Kepler (Borucki et al. 2010) and K2 (Howell et al. 2014) fields has uncovered their evolutionary stages (e.g., Stello et al. 2013; Mosser et al. 2015; Vradar et al. 2016; Hon et al. 2018; Zinn et al. 2020). Particularly, based on the asteroseismic scaling relations, the positions of the RGB bump as well as the zero-age sequence of HeB (ZAHeB) stars could be well defined in a mass–radius diagram (Li et al. 2021). Deepak & Lambert (2021) explored the evolution of lithium in giant stars based on ~ 200 seismic data. Based on the distribution of A_{Li} as a function of mean large frequency separation ($\Delta\nu$), they found no indication of Li enrichment near the luminosity bump. Martell et al. (2021) explored the properties of 1262 Li-rich giant stars from the GALAH (De Silva et al. 2015) and K2 surveys and found that the less massive primary red clump stars are 1.5 times more likely to be super lithium-rich than the more massive secondary red clump stars. Differing from the result shown in Deepak & Lambert (2021), Martell et al. (2021) showed that there is a concentration of lithium-rich stars near the luminosity of the red giant branch bump. Recently, thousands of stars in the Kepler and K2 fields have been observed by the Large Sky Area Multi-Object Fibre Spectroscopic Telescope (LAMOST) spectroscopic survey (Zhao et al. 2006; Cui et al. 2012; Zhao et al. 2012) and their surface Li abundances have been presented recently (Gao et al. 2019, 2021). Combining these data sets, it is possible for us to investigate the signatures of Li abundances for stars evolving from the RGB to the HeB phase. Also, it would shed light on the Li production in evolved stars and give more detailed insight into the nature of stellar evolution theory.

In this Letter, we characterize signatures of Li abundances for giant stars at different evolutionary stages observed by both LAMOST and Kepler (K2 included). In Section 2, we introduce the sample selection. In Section 3, we estimate the mass and radius of our sample stars and characterize the evolutionary features of Li abundances in different stages. We summarize our results in Section 4.

2. Stellar Samples

Gao et al. (2019) searched for Li-rich giants using the LAMOST low-resolution spectra, and they found 10,535 giant stars with $A_{\text{Li}} \geq 1.5$ dex. This catalog provided the updated largest sample of Li-rich giants. Very recently, Gao et al. (2021) further determined Li abundances for a sample of 165,479 stars based on the LAMOST medium-resolution spectra. We thus considered the two catalogs as our initial targets and cross matched the combined catalog with these of Yu et al. (2018) and Zinn et al. (2020). The latter two catalogs provided the frequency of maximum power (ν_{max}), the mean large frequency separation ($\Delta\nu$) and the classification of evolutionary stages for samples of 16,094 giants in the Kepler field and of 4395 giants in the K2 fields, respectively. A total of 1848 giant stars are finally selected, including 904 RGB stars and 944 HeB stars. Among them, there are 30 stars that have detected Li abundances both in the low- and medium-resolution observational modes and the Li results from medium-resolution modes are adopted in this work. Because of the way these stars were selected, we do not try to address the detection fractions of Li-rich stars here. However, we do note that Li was detected in $\sim 80\%$ of the sample with no strong trends in detection fraction as a function of mass, metallicity, or evolutionary state likely to bias our analysis.

3. Li Abundances in M - R Diagram

It has been proved that asteroseismic parameters ($\Delta\nu$, ν_{max}) are tightly related to stellar fundamental parameters and stellar masses and radii can be estimated by asteroseismic parameters with an addition of effective temperature (T_{eff}), also known as the asteroseismic scaling relations (see, e.g., Stello et al. 2008; Kallinger et al. 2010, and references therein). These relations have also been confirmed, having remarkable constraining powers with intrinsic scatter of mass and radius being limited to $\sim 1.7\%$ and $\sim 0.4\%$, respectively (Li et al. 2021). Taking advantage of these asteroseismic scaling relations, we can construct a mass-radius diagram (hereafter, M - R diagram) instead of a traditional Hertzsprung-Russell diagram to investigate the evolutionary features of Li abundances in evolved stars. We calculate the mass and radius of our sample following

$$\frac{M}{M_{\odot}} \approx \left(\frac{\nu_{\text{max}}}{f_{\nu_{\text{max}}} \nu_{\text{max},\odot}} \right)^3 \left(\frac{\Delta\nu}{f_{\Delta\nu} \Delta\nu_{\odot}} \right)^{-4} \left(\frac{T_{\text{eff}}}{T_{\text{eff},\odot}} \right)^{3/2}, \quad (1)$$

$$\frac{R}{R_{\odot}} \approx \left(\frac{\nu_{\text{max}}}{f_{\nu_{\text{max}}} \nu_{\text{max},\odot}} \right) \left(\frac{\Delta\nu}{f_{\Delta\nu} \Delta\nu_{\odot}} \right)^{-2} \left(\frac{T_{\text{eff}}}{T_{\text{eff},\odot}} \right)^{1/2}, \quad (2)$$

where, $\nu_{\text{max},\odot} = 3090 \mu\text{Hz}$, $\Delta\nu_{\odot} = 135.1 \mu\text{Hz}$, and $T_{\text{eff},\odot} = 5777 \text{ K}$ (Huber et al. 2011). The parameters $f_{\nu_{\text{max}}}$ and $f_{\Delta\nu}$ are correction factors. Following Sharma et al. (2016), the factor $f_{\Delta\nu}$ is a function of stellar atmospheric parameters (T_{eff} , $\log g$, $[\text{Fe}/\text{H}]$) and evolutionary phase and can be determined by interpolation in

grids of models for $-3 > [\text{Fe}/\text{H}] < 0.4$ and $0.8 < M/M_{\odot} < 4.0$. Since the factor $f_{\nu_{\text{max}}}$ is difficult to be determined theoretically (Belkacem et al. 2011), it was set to be 1.0 in this work. The stellar atmospheric parameters were adopted from Gao et al. (2019) and Gao et al. (2021). The $\Delta\nu$ and ν_{max} for stars in the K2 fields were adopted from the mean values of different pipelines (Zinn et al. 2020), while for stars in the Kepler field they were determined via the SYD pipeline (Yu et al. 2018). The small differences in mass and radius determined by different pipeline results would not affect our mapping of lithium evolution.

3.1. Li Abundances in RGB Stars

To better understand the evolutionary features of Li abundances and the origin of Li enhancement in evolved stars, we separate HeB from RGB for our sample stars and characterize Li abundances for each population. Figure 1 shows the M - R diagrams of the RGB (panel a) and HeB (panel c) stars in our sample color-coded by Li abundances as well as the Li abundance versus radius for low-mass RGB stars (panel b). The red line in panel (a) defines the RGB bump, while the gold spline in panel (c) indicates the zero-age HeB (ZAHeB) edge (see Li et al. 2021 for details).

As shown in Figure 1(b), for the majority of low-mass ($M < 2M_{\odot}$) RGB stars, the Li abundances decrease gradually by ~ 2.0 dex when their radii expand by a factor of ~ 5 . This feature indicates the consequence of Li depletion along with stellar evolution, which has been predicted by the standard stellar evolution theory (e.g., Iben 1967). As shown in Figure 1(a), there are no obvious crowd stars with anomalously high Li abundances near the bump. Considering the definition of $A_{\text{Li}} \geq 1.5$ dex for Li-rich stars, the total number of these stars among low-mass RGB accounts for 45, while only 5 of them evolve past the bump. This result implies that the RGB bump may be not the key to Li enhancement of RGB stars. A similar result was reported by Deepak & Lambert (2021), who found no indication of Li enrichment near the luminosity bump. As suggested by previous studies (e.g., Yan et al. 2021), these Li-rich stars may possess higher A_{Li} than their counterparts at main-sequence stage; they could also still reserve relatively high A_{Li} after finishing the FDU process. Therefore, the Li-rich RGB stars might be a natural consequence of Li depletion along with stellar evolution. Given that the depletion of Li by the FDU process is generally with a factor of ~ 60 (Iben 1967), if we take a low-mass sample star with the highest A_{Li} of ~ 2.4 dex below the bump, the A_{Li} would be up to ~ 4.2 dex at the main-sequence stage. Such stars have been reported by previous studies (e.g., Li et al. 2018; Gao et al. 2021). The external scenario, on the other hand, such as engulfment of a substellar component (e.g., Alexander 1967; Siess & Livio 1999), cannot be excluded, which is in accordance with the observed Li abundances for our Li-rich RGB stars. A simulation of engulfment of a Jovian planet can result in a typical upper limit of $A_{\text{Li}} \sim 2.2$ dex (Aguilera-Gómez et al. 2016), which is sufficient for Li production in most Li-rich stars in our sample that are below the bump.

As mass increases, we found that Li abundances are comparably higher. Although intermediate-mass RGB stars show Li depletion like that of low-mass RGB objects, the depletion is moderate. In fact, the thinner convective envelope in intermediate-mass RGB stars is usually accompanied by relatively lower temperature in the deep convection zone and

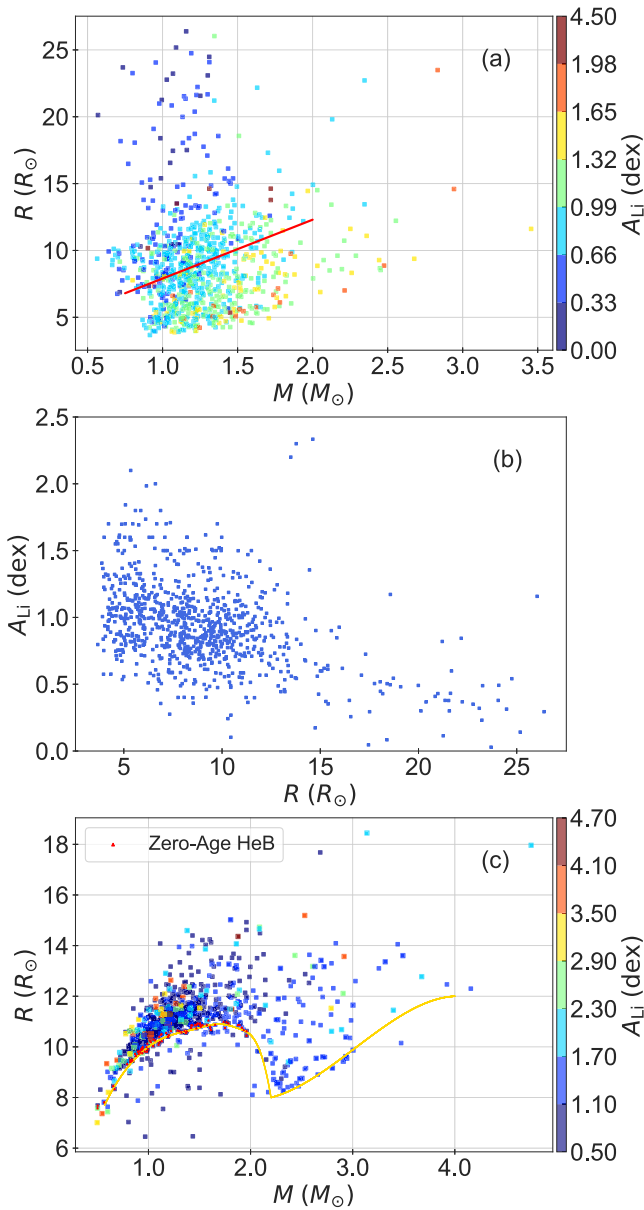


Figure 1. Radius vs. mass for RGB (upper) and HeB (lower) stars color-coded by Li abundance as well as radius vs. Li abundance for low-mass RGB stars (middle). The red line in the upper panel denotes the RGB bump. The gold spine in the lower panel denotes the edge of ZAHHeB stars and the red triangles denote the stars locating within reach of ZAHHeB edge.

shorter time available for deep mixing, on which the destruction of Li is dependent. As a result, high Li abundance can be easily found among intermediate-mass RGB stars.

3.2. Li Abundances in HeB Stars

After leaving the tip of the RGB (tip-RGB) phase, stars evolve down in luminosity and begin core helium burning (HeB), which is also known as the red clump phase. The low-luminosity edge defines the beginning of the red clump, which is also called the zero-age HeB (ZAHHeB) phase. The edge is evident in H–R diagrams as well as in M – R diagrams (Girardi 2016; Li et al. 2021), which makes it feasible to look into the evolutionary features of Li abundance among HeB stars. In Figure 1(c), this edge is visible as the lower boundary.

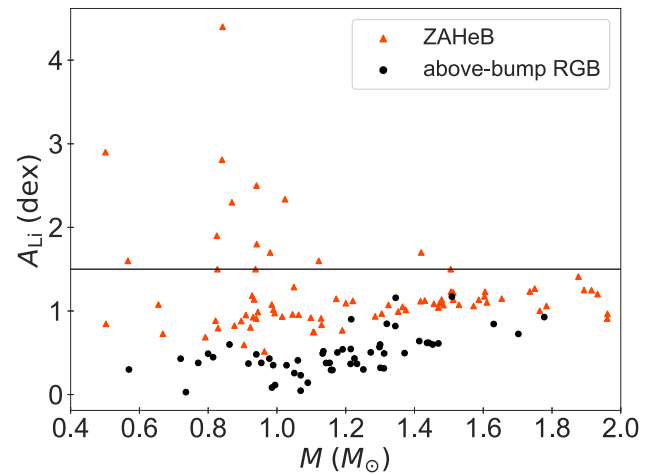


Figure 2. Li abundances vs. mass for stars locating above the RGB bump and HeB stars within reach of the ZAHHeB edge. The horizontal line denotes the lower limit of Li enhancement.

As shown in Figure 1(c), the HeB stars possess a high frequency of Li-rich stars whose Li abundances are higher than the primordial abundance (Cyburt et al. 2016). Moreover, most of these stars are dominated by low-mass stars. Interestingly, the radii of these stars are distributed over a wide range and do not show any significant feature, which indicates that the super Li-rich stars can be found at anytime during the steady-state phase of core helium burning.

According to some recent studies, the helium-flash-induced mixing event occurs between tip-RGB and HeB phases, which is proposed to be responsible for Li enhancement among low-mass HeB stars (see Kumar et al. 2020; Schwab 2020, and references therein). Since low-mass ZAHHeB stars could be well defined for our sample, one would expect to see a significant increase of A_{Li} for these stars in comparison with that for stars at or near tip-RGB based on the scenario of helium-flash-induced mixing. Considering the asteroseismic measurements and inferences become less certain at large radii (Pinsonneault et al. 2018), we further select a subset of low-mass RGB stars with their radii greater than $15R_{\odot}$ (Figure 1(a)), we consider them to be above-bump RGB stars. Then, we select the other subset of low-mass HeB stars, locating within reach of the ZAHHeB edge (Figure 1(c)). We present the Li abundance versus mass for the two subsets in Figure 2. It can be seen that most ZAHHeB stars have higher Li abundances than those of stars above the bump. The median A_{Li} increases by ~ 0.6 dex from post-bump to ZAHHeB phase. This increment is very close to the result given by the model prediction after including the helium-flash-induced mixing (see their Figure 3 in Schwab 2020), which means that the scenario of helium-flash-induced mixing indeed contributes Li production for most low-mass HeB stars. The increment shown in our sample provides observational evidence for Li production due to helium-flash-induced mixing. However, the A_{Li} of the majority of ZAHHeB stars are close to 1.0 dex, which hardly meets the traditional standard of Li-rich giants. For these Li-rich low-mass HeB stars, we suggest that some special physical mechanisms should be needed during the helium flash so that abnormal enhancement of Li could be triggered. Another possible interpretation for these Li-rich low-mass HeB stars is the merger of a helium white dwarf (HeWD) with an RGB star (Zhang et al. 2020). The HeWDRGB merger could result in a

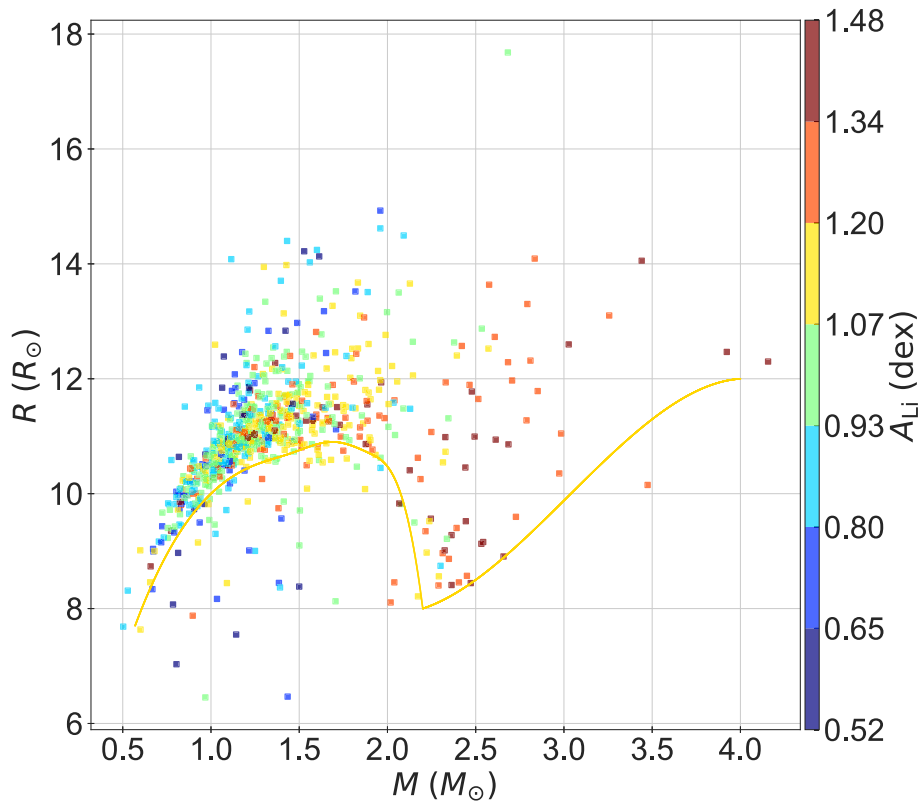


Figure 3. Same as Figure 1(c), but showing HeB stars with $A_{\text{Li}} < 1.5$.

Li-rich HeB star at anytime during the HeB star’s steady-state phase of core He burning (Zhang et al. 2020), which is compatible with the observational distribution of our sample. Yan et al. (2021) showed that the HeWDRGB merger scenario generally agrees with the observed Li abundances in their sample stars. Our results do not support the proposal of Singh et al. (2021) who used variations of asymptotic gravity-mode period spacing ($\Delta\Pi$) as a tracer of duration for core helium burning and found that the super Li-rich giants are almost exclusively young HeB stars. Although in this work we could not define the upper edge of HeB in the M – R diagram, the Li-rich low-mass HeB stars with large radii are supposed to be evolved HeBs.

The features of Li-rich HeB stars indeed provide clues to understand stellar internal physical processes, however, they are just a small fraction of evolved stars. To give a more explicit picture for Li evolution, we focused on those HeB stars with A_{Li} less than 1.5 dex, which we referred to as Li-normal HeB stars. We plot the M – R diagram only for the Li-normal HeB stars in Figure 3. On one hand, it can be seen that the Li abundances strongly relate to the stellar masses, with higher-mass stars possessing higher Li abundances. As a whole, the intermediate-mass stars have a median A_{Li} of 1.3 dex, which is 0.3 dex higher than that of the low-mass stars. This relation is also attributed to the thinner convective envelope in higher-mass stars, which weakens the depletion of Li. On the other hand, there is no obvious sign of decreasing A_{Li} along with radii; this feature can be justified for stars at the red clump phase which would not be affected by further mixing because the retreat of the convective envelope causes it to remain rather far from the H-burning shell at this evolutionary stage (Palmerini et al. 2011).


4. Conclusions

In this Letter, we investigate the evolutionary features of Li for a sample of stars evolved from the RGB to the HeB stage in the LAMOST-Kepler/K2 project. The RGB stars show a Li depletion feature along with stellar evolution. The Li-rich RGB stars mainly locate below the bump, and there are no obvious crowd stars with anomalously high Li abundances near the bump, which indicates that Li-rich RGB stars might be a natural consequence of Li depletion along with stellar evolution. We found an immediate increase of Li abundance by ~ 0.6 dex for stars between the post-bump of RGB and the ZAHB phase, which suggests that helium flash can be responsible for moderate production of Li. This increment provides observational evidence for Li production due to helium-flash-induced mixing events. Furthermore, we found that Li-rich HeB stars locate anywhere during the HeB stars’ steady-state phase of core He burning. We suggest that either some special physical mechanisms should be required in helium flash for vigorous Li production or they are formed via other scenarios that could result in random distributions in the HeB phase. In addition, during the HeB stage, we found the depletion feature of Li is not obvious for stars with A_{Li} less than 1.5 dex, which would be a visible manifestation of the convective envelope retreating as well as an inefficient deep-mixing process inside HeB stars.

We thank the referee for the thorough reviews that have helped us to improve the manuscript. This work is supported by the National Key R&D Program of China No.2019YFA0405502 and the National Natural Science Foundation of China under grant Nos. 12090040, 12090044, 12022304, U2031203, 11833006, 11973052, 11973042, 11988101, 11890694 and U1931102.

H.-L.Y. acknowledges support from the Youth Innovation Promotion Association of the CAS (id. 2019060) and NAOC Nebula Talents Program. We acknowledge the entire Kepler team and everyone involved in the Kepler mission. Funding for the Kepler Mission is provided by NASA's Science Mission Directorate. Guoshoujing Telescope (the Large Sky Area Multi-Object Fiber Spectroscopic Telescope, LAMOST) is a National Major Scientific Project built by the Chinese Academy of Sciences. Funding for the project has been provided by the National Development and Reform Commission. LAMOST is operated and managed by the National Astronomical Observatories, Chinese Academy of Sciences.

ORCID iDs

Jinghua Zhang  <https://orcid.org/0000-0002-2510-6931>
 Jian-Rong Shi  <https://orcid.org/0000-0002-0349-7839>
 Hong-Liang Yan  <https://orcid.org/0000-0002-8609-3599>
 Yaguang Li  <https://orcid.org/0000-0003-3020-4437>
 Qi Gao  <https://orcid.org/0000-0003-4972-0677>
 Chun-Qian Li  <https://orcid.org/0000-0002-6647-3957>
 Xianfei Zhang  <https://orcid.org/0000-0002-3672-2166>
 Shaolan Bi  <https://orcid.org/0000-0002-7642-7583>
 Gang Zhao  <https://orcid.org/0000-0002-8980-945X>
 Yan Li  <https://orcid.org/0000-0002-1424-3164>

References

- Aguilera-Gómez, C., Chanamé, J., Pinsonneault, M. H., & Carlberg, J. K. 2016, *ApJL*, **833**, L24
- Alexander, J. B. 1967, *Obs*, **87**, 238
- Belkacem, K., Goupil, M. J., Dupret, M. A., et al. 2011, *A&A*, **530**, A142
- Borucki, W. J., Koch, D., Basri, G., et al. 2010, *Sci*, **327**, 977
- Casey, A. R., Ho, A. Y. Q., Ness, M., et al. 2019, *ApJ*, **880**, 125
- Charbonnel, C., & Lagarde, N. 2010, *A&A*, **522**, A10
- Cui, X.-Q., Zhao, Y.-H., Chu, Y.-Q., et al. 2012, *RAA*, **12**, 1197
- Cyburt, R. H., Fields, B. D., Olive, K. A., & Yeh, T.-H. 2016, *RvMP*, **88**, 015004
- De Silva, G. M., Freeman, K. C., Bland-Hawthorn, J., et al. 2015, *MNRAS*, **449**, 2604
- Deepak, & Lambert, D. L. 2021, *MNRAS*, **505**, 642
- Deepak, & Reddy, B. E. 2019, *MNRAS*, **484**, 2000
- Deliyannis, C. P., Anthony-Twarog, B. J., Lee-Brown, D. B., & Twarog, B. A. 2019, *AJ*, **158**, 163
- Gao, Q., Shi, J.-R., Yan, H.-L., et al. 2019, *ApJS*, **245**, 33
- Gao, Q., Shi, J.-R., Yan, H.-L., et al. 2021, *ApJ*, **914**, 116
- Girardi, L. 2016, *ARA&A*, **54**, 95
- Hon, M., Stello, D., & Yu, J. 2018, *MNRAS*, **476**, 3233
- Howell, S. B., Sobek, C., Haas, M., et al. 2014, *PASP*, **126**, 398
- Huber, D., Bedding, T. R., Stello, D., et al. 2011, *ApJ*, **743**, 143
- Iben, Icko, J. 1967, *ApJ*, **147**, 624
- Kallinger, T., Weiss, W. W., Barban, C., et al. 2010, *A&A*, **509**, A77
- Kumar, Y. B., Reddy, B. E., Campbell, S. W., et al. 2020, *NatAs*, **4**, 1059
- Li, H., Aoki, W., Matsuno, T., et al. 2018, *ApJL*, **852**, L31
- Li, Y., Bedding, T. R., Stello, D., et al. 2021, *MNRAS*, **501**, 3162
- Lind, K., Primas, F., Charbonnel, C., Grundahl, F., & Asplund, M. 2009, *A&A*, **503**, 545
- Martell, S. L., Simpson, J. D., Balasubramanian, A. G., et al. 2021, *MNRAS*, **505**, 5340
- Mori, K., Kusakabe, M., Balantekin, A. B., Kajino, T., & Famiano, M. A. 2021, *MNRAS*, **503**, 2746
- Mosser, B., Vrad, M., Belkacem, K., Deheuvels, S., & Goupil, M. J. 2015, *A&A*, **584**, A50
- Palmerini, S., Cristallo, S., Busso, M., et al. 2011, *ApJ*, **741**, 26
- Pinsonneault, M., Elsworth, Y., Silva Aguirre, V., et al. 2018, AAS Meeting, **231**, 450.13
- Randich, S., & Magrini, L. 2021, *FrASS*, **8**, 6
- Schwab, J. 2020, *ApJL*, **901**, L18
- Sharma, S., Stello, D., Bland-Hawthorn, J., Huber, D., & Bedding, T. R. 2016, *ApJ*, **822**, 15
- Siess, L., & Livio, M. 1999, *MNRAS*, **308**, 1133
- Singh, R., Reddy, B. E., Campbell, S. W., Kumar, Y. B., & Vrad, M. 2021, *ApJL*, **913**, L4
- Smiljanic, R., Franciosini, E., Bragaglia, A., et al. 2018, *A&A*, **617**, A4
- Stello, D., Bruntt, H., Preston, H., & Buzasi, D. 2008, *ApJL*, **674**, L53
- Stello, D., Huber, D., Bedding, T. R., et al. 2013, *ApJL*, **765**, L41
- Twarog, B. A., Anthony-Twarog, B. J., Deliyannis, C. P., & Steinhauer, A. 2020, *MmSAI*, **91**, 74
- Vrad, M., Mosser, B., & Samadi, R. 2016, *A&A*, **588**, A87
- Wallerstein, G., & Sneden, C. 1982, *ApJ*, **255**, 577
- Yan, H.-L., Shi, J.-R., Zhou, Y.-T., et al. 2018, *NatAs*, **2**, 790
- Yan, H.-L., Zhou, Y.-T., Zhang, X., et al. 2021, *NatAs*, **5**, 86
- Yu, J., Huber, D., Bedding, T. R., et al. 2018, *ApJS*, **236**, 42
- Zhang, X., Jeffery, C. S., Li, Y., & Bi, S. 2020, *ApJ*, **889**, 33
- Zhao, G., Chen, Y.-Q., Shi, J.-R., et al. 2006, *ChJAA*, **6**, 265
- Zhao, G., Zhao, Y.-H., Chu, Y.-Q., Jing, Y.-P., & Deng, L.-C. 2012, *RAA*, **12**, 723
- Zinn, J. C., Stello, D., Elsworth, Y., et al. 2020, *ApJS*, **251**, 23